Int. J. Heat Mass Transfer. Vol. 9, pp. 1297–1320. Pergamon Press 1966. Printed in Great Britain

HEAT-TRANSFER AND FRICTION PROPERTIES OF SURFACES WITH DISCRETE ROUGHNESSES

N. SHERIFF and P. GUMLEY
UKAEA, Reactor Group, Risley, Warrington, Lancs.

(*Received* 29 *July* 1965 *and in revised form* 7 *March* 1966)

Abstract—The heat-transfer and friction characteristics of a surface with discrete roughnesses have been investigated experimentally.

The surfaces were roughened by means of a wire wrapping at a constant pitch-to-wire diameter ratio of 10:1, with wire sizes varying from 0·002- to 0·040-in dia.

A simple correlation on the basis of a non-dimensional roughness parameter e^+ was found to be useful, but a more exact correlation on the basis of a two-layer model of the heat-transfer resistance was more exact. In this model the heat-transfer process was sub-divided into a region from the wall to the envelope enclosing the roughness tips, and a central core region.

The heat-transfer resistance from the wall to the roughness tips has a minimum value at $e^+ \sim 35$, and this produces an optimum heat-transfer surface.

NOMENCLATURE

A, constant in rough-surface velocity profile;
c, specific heat;
e, roughness height;
e^+, dimensionless roughness parameter, $e\sqrt{(\tau/\rho)}\nu$;
f, fanning friction coefficient;
k, thermal conductivity;
h, mean heat-transfer coefficient;
h_w, wall heat-transfer coefficient, $q/(t_w - t_1)$;
q, heat flux;
Pr, Prandtl number;
Re, Reynolds number;
St, Stanton number, $h/\rho uc$;
St_w, wall Stanton number, $h_w/\rho u_\tau c$;
t, temperature;
t^+, dimensionless temperature, $t/(q_w/\rho u_\tau c)$;
u, fluid velocity;
u_τ, friction velocity, $\sqrt{(\tau/\rho)}$;
u^+, dimensionless velocity, $u/\sqrt{(\tau/\rho)}$;
y, distance from the wall;
y^+, dimensionless distance parameter, $y\sqrt{(\tau/\rho)}/\nu$;
τ, shear stress;
ρ, density;
ν, kinematic viscosity;
ϵ_M, eddy diffusivity of momentum;
ϵ_H, eddy diffusivity of heat;
δm, correction to allow for differences between velocity and temperature distribution [see equation (3)].

Subscripts

1 evaluated at boundary between régimes in roughened channel;
m, evaluated at maximum velocity position;
e, evaluated at roughness tip;
0, mean value;
w, evaluated at the wall;
R, roughened surface;
s, smooth surface.

INTRODUCTION

1. There have been many heat-transfer investigations involving roughened surfaces since the initial work of Cope [1]. Most of these studies have been made in the past twelve years and inspired mainly by nuclear reactor applications. The improved heat-transfer performance of roughened surfaces enables the reactor rating to be increased for a given size, and the capital

cost per unit sent out reduced. The types of roughnesses have varied, from machined threads to wires close to the surface, as have also the flow geometries. Table 1 lists the major works, showing the differing geometries and roughness configurations.

2. The emphasis of the various investigations naturally has depended on the principal objectives. For example, the studies of Sams [2, 3], Draycott and Lawther [4] and Walker and Rapier [5] were directed to optimizing the heat-transfer surface of a fuel element. Consequently comprehensive testing of various roughened surfaces was necessary; in particular Draycott and Lawther studied twenty-one different surfaces. In contrast, Nunner and Dipprey and Sabersky used semi-theoretical arguments to explain the effects of roughened surfaces on the heat-transfer coefficient [6, 7]. The work of Dipprey and Sabersky involved a study of the heat-transfer properties of surfaces similar to those used by Nikuradse in his historic work on roughened surfaces [8]. Owen and Thomson simultaneously with Dipprey and Sabersky produced a similar analysis [9]. In both analyses an assumption as to the flow and mechanism of heat removal in the wall region was necessary. Experimental results on the local heat-transfer coefficient for roughened surfaces help to fill this gap, and are provided by references [10] and [11]. The main feature of these experiments was the measurement of the heat-transfer rate between the discrete roughnesses, in one case with a direct heat-transfer experiment and in the other with a mass-transfer analogue.

3. In addition to these heat-transfer studies, Savage and Myers investigated the loss characteristics of finned surfaces [12]. They studied the pressure distribution around rectangular fins for various pitches and thus divided the loss into its two components, friction and form drag. One pertinent conclusion from their results is that the friction resistance is a minimum at a pitch-to-height ratio of about 10, which is the value used in the present investigation.

4. This brief guide to the main studies shows that the field of roughened-surface heat-transfer is already extensive. The present work was an attempt at a general correlation for one particular roughness configuration, i.e. circular in shape and with a constant pitch-to-diameter ratio. If such a correlation proved possible the data could be used more flexibly by designers, and less experimental work would be needed to study similar configurations in the future.

Table 1. Roughened-surface heat-transfer studies

Investigators	Geometry	Type of roughness	Fluid	Reynolds number range	Number of surfaces
Nunner [6]	circular tube	semi-circular, rectangular	air	10^3–7×10^4	8
Dipprey and Sabersky [7]	circular tube	sand grain	water	2×10^4 5×10^5	4
Edwards and Sheriff [10]	rectangular duct	wire	air	2×10^5	8
Sams [2, 3]	circular tube	machined square-thread and wire	air	10^4–2×10^5 7×10^3–7×10^4	3 sq. thread 14 wire
Walker and Rapier [5]	annulus	machined rectangular	air	$\sim 2 \times 10^5$	17
Draycott and Lawther [4]	annulus	machined square and thread, wire-wound	air	4×10^4–4×10^5	21
Lancet [21]	rectangular duct	numerous finite protrusions	air	4×10^3–3×10^4	1
Fournel [20]	rectangular duct	wire	air	$1{\cdot}7 \times 10^4$–5×10^4	2
This work	annulus	wire	air	10^4–2×10^3	6

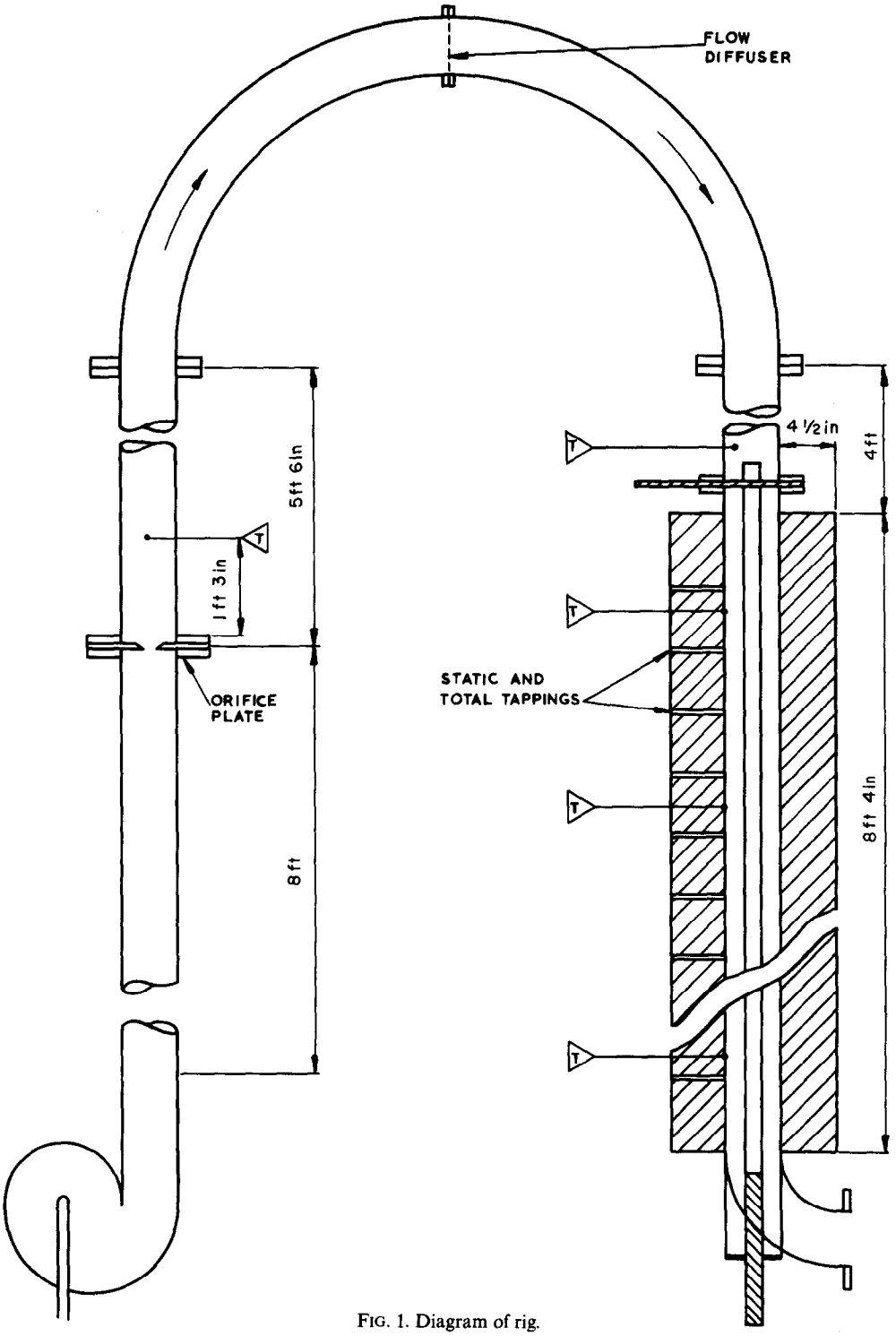

FIG. 1. Diagram of rig.

EXPERIMENTAL RIG AND PROCEDURE

5. The rig consisted essentially of an air blower leading to a vertical measuring section, which was followed after a bend of 180° by the test section. The test section was an annular flow passage formed by a central stainless-steel heater tube of 1·03-in o.d., with the inside diameter of the main pipework 3·13 in. The length of the test section was approximately 100 in, giving a length-to-equivalent-diameter ratio of about 50. Surrounding the test section was a layer, 4-in thick, of regranulated cork for insulation. Fig. 1 shows the rig diagrammatically.

6. Electricity was supplied to the heater tube from the transformer via a specially machined copper flange at the top and a copper rod at the bottom. Both these connections were shrunk-fitted to the heater tube, which was machined from 0·75-in-n.b. stainless-steel tubing. Details of the heater tube are shown in Fig. 2.

7. Most of the instrumentation of the rig was centred on the heater tube, to which were spot-welded, on the inside, 21 Chromel–Alumel thermocouples and four voltage tappings. The current was measured via a current transformer, and the power evaluated using the measured resistance of the heater and measured temperature coefficient of resistance. The thermocouples and voltage tappings were brought out of the heater tube through slots at the lower end. Other instrumentation included a suction pyrometer for the inlet air temperature measurement and four thermocouples on the outside of the outer tube of the annulus. Pressure tappings at 10-in intervals along the test section and positions for velocity and temperature transverses were also included. The total flow was measured by an orifice plate in the section upstream of the test section.

8. The roughened surfaces were produced by wrapping wire tightly around the heater tube (Fig. 3). The wire was chosen so that it had a slightly lower coefficient of expansion than the tube, and any tendency to become loose when heated was reduced. The geometry of the roughened surfaces was such that the pitch-to-height ratio was maintained at 10. The accuracy of the winding was checked by a shadow enlargement of the surface, which revealed that the mean spacing of the surfaces varied from 9·9 to 10·5 between tubes with a mean standard deviation of $\pm 0{\cdot}5$. Altogether six roughness sizes were studied, viz. 0·040, 0·0285, 0·020, 0·010, 0·005 and 0·002 in in dia.

9. The several preliminary tests and measurements made will be dealt with briefly. The wide flow range of the experiment involved the use of two orifice plates, and to ensure a reliable overlap they were calibrated against a velocity transverse. A flow straightener in the form of a shaped gauge was placed in the 180° bend to ensure a uniform flow distribution in the test section. Static heat tests were made to calibrate the thermocouples on the outside of the outer tube of the annulus in terms of heat loss from the test section. From the same tests the effective emissivity from the heater to the outer tube was assessed and the contribution of the heat loss by radiation under conditions of forced convection was small. The inlet air thermocouple measurement was calibrated against the wall thermocouples to reduce temperature errors.

10. The procedure for each test is now so standard that details will not be given here; it is worth noting, however, the method used to evaluate the heat-transfer coefficients. A typical test result is shown in Fig. 4, indicating the variation of the surface temperature along the channel length and the inlet gas temperature. Allowance has been made for the radial temperature drop through the heater wall. From the heat flux, mass flow and heat loss the bulk gas temperature rise can be evaluated, and the line through the inlet gas temperature shows the rate of rise of the gas temperature. From a distance along the heater of about 30 in, the temperature difference between the heater surface and the bulk gas temperature does not vary appreciably for the remainder of the heater length. The temperature difference used to evaluate the heat-transfer coefficient was the mean of all the surface-to-bulk

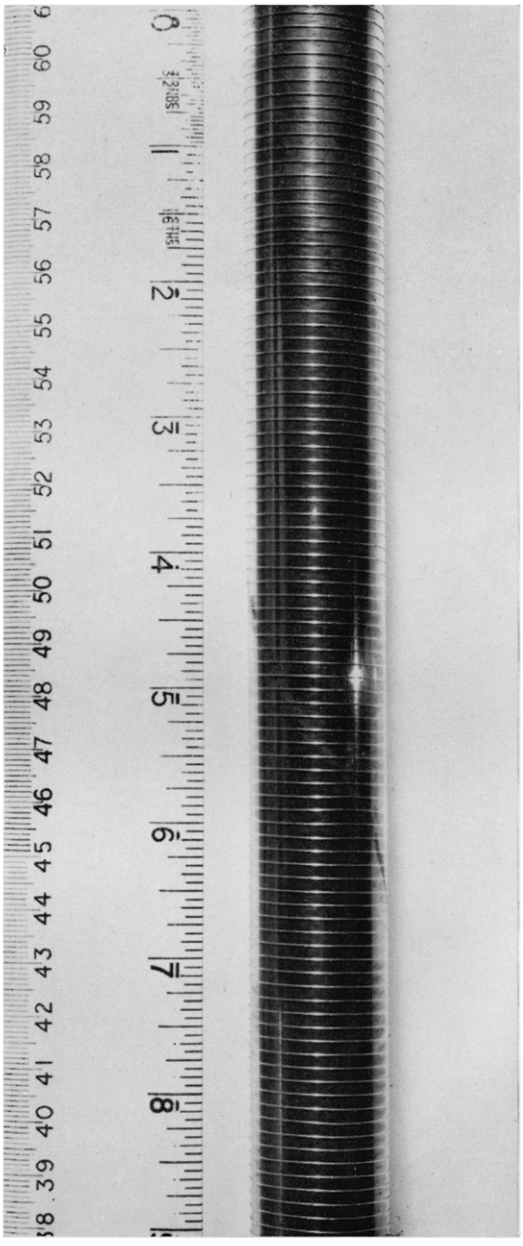

FIG. 3. A typical wire-wound test surface.

[*facing page 1300*]

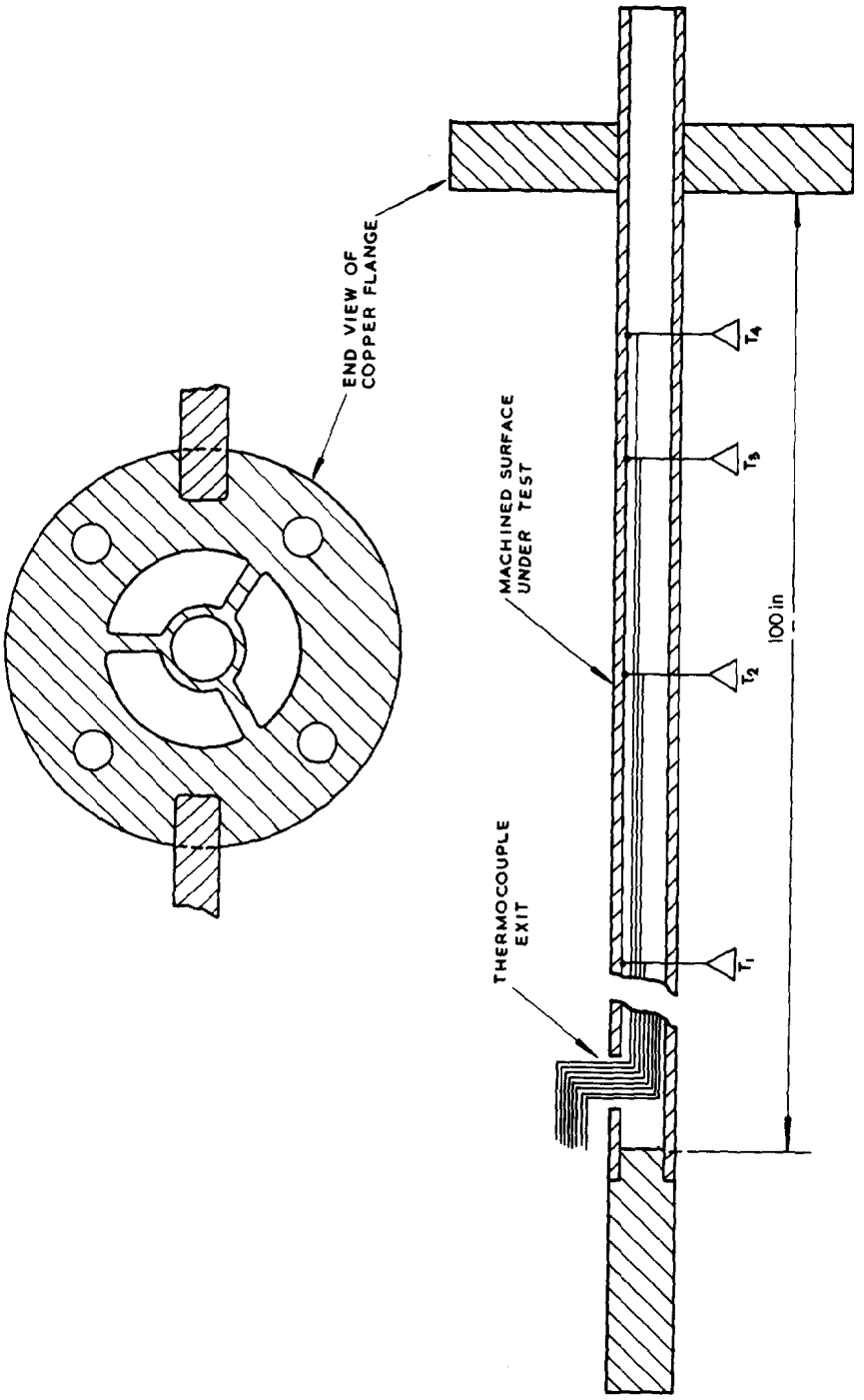

FIG. 2. Heater tube details.

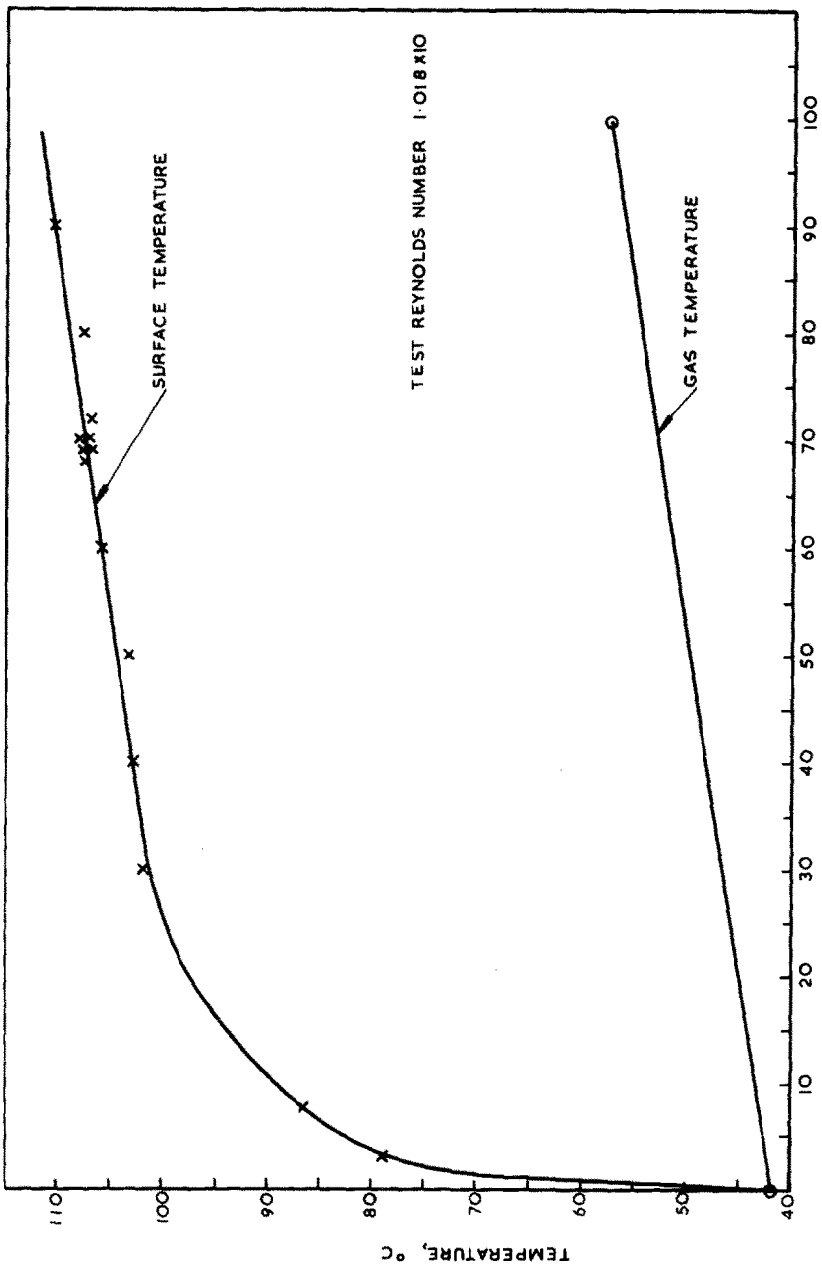

FIG. 4. Heater temperature distribution in typical test.

temperature differences in this region of nominally constant temperature difference.

11. In general, about eleven thermocouple readings were used to evaluate the mean temperature difference. The root-mean-square deviation from the mean was never greater than 2 per cent, and in most cases was about 1 per cent. Temperature variations around the heater were checked from three thermocouples all at the same axial position but spaced 120° apart. The temperature variations measured were about 1 per cent of the surface-to-bulk temperature difference, and represent a combination of heater wall-thickness variation and asymmetric cooling of the heater.

RESULTS

Heat transfer and friction

12. The range of Reynolds number used was 10^4 to 2×10^5, and the conventional plot of Nusselt number against Reynolds number is shown in Fig. 5. The effective diameter used was based on an annulus with the inner surface taken as the cylinder enveloping the roughness peaks. The same surface was used for the heat-transfer area. Comparison of the smooth annular data with a recent semi-theoretical analysis [13] gives an agreement to within 10 per cent at the higher Reynolds numbers.

13. The presentation of annular heat-transfer and friction results based on the equivalent

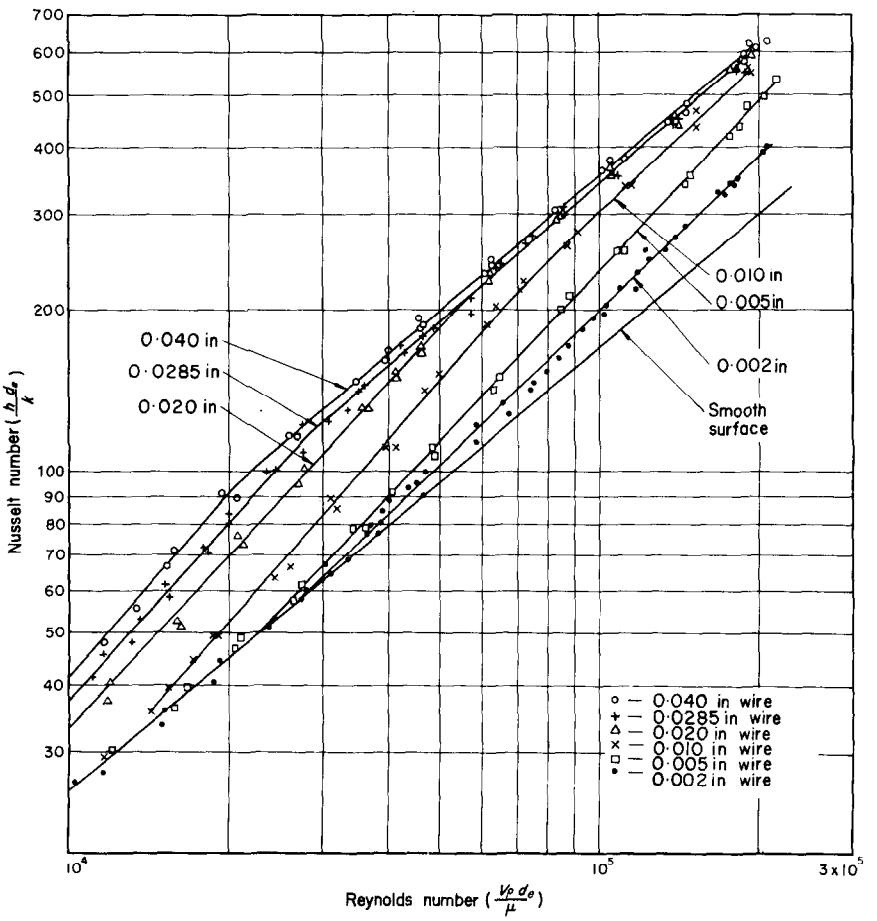

FIG. 5. Conventional Nusselt number against Reynolds number.

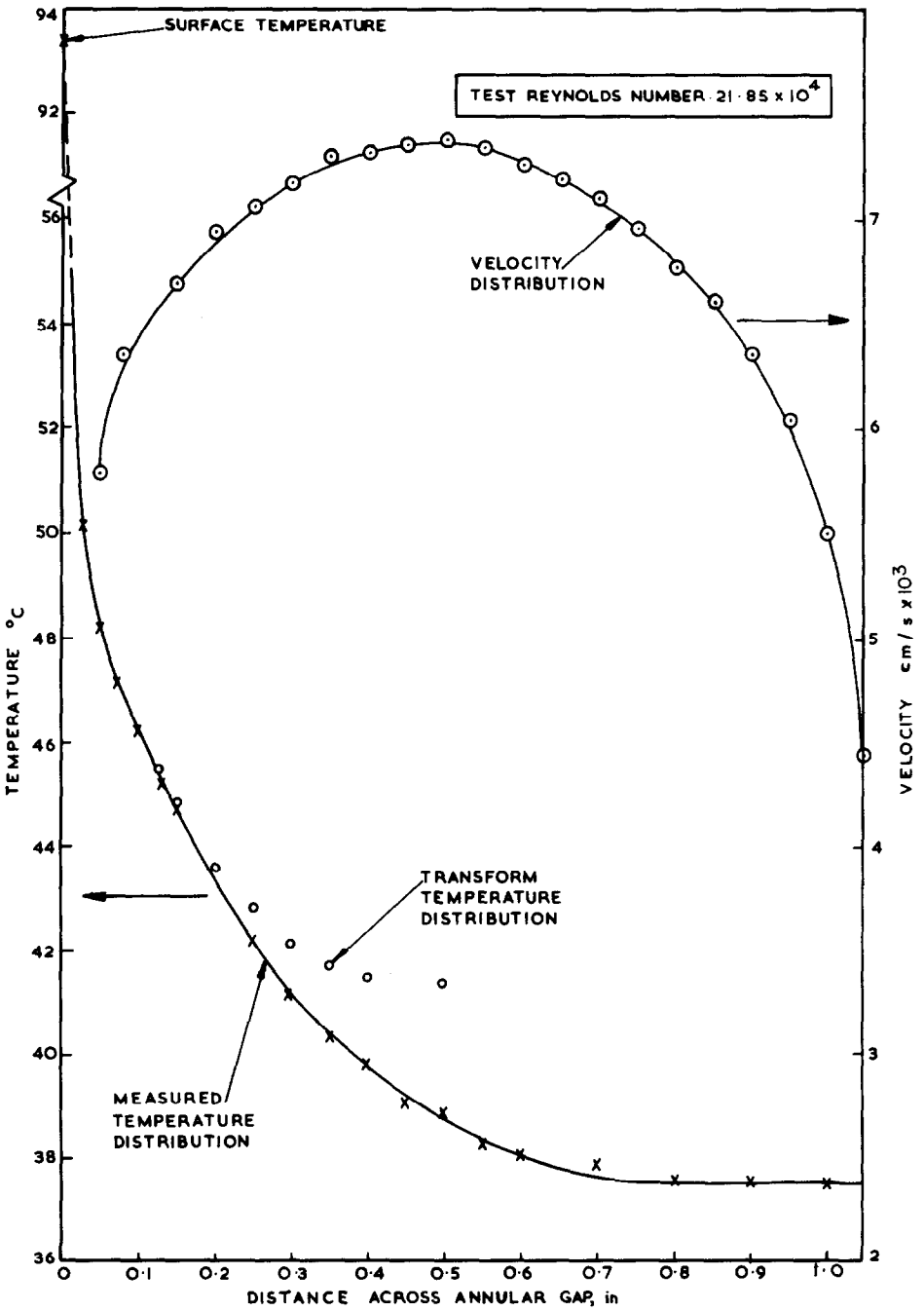

FIG. 6. Measured temperature and velocity distributions; transformed temperature distribution.

diameter of the annulus is not completely satisfactory, particularly with only the inner diameter of the annulus being both roughened and heated. To allow for this, Hall introduced a transformation in which he treated the flow passage as two distinct regions on either side of the radius of zero shear, and made the heat flux zero at the position of zero shear [14]. This made the boundary conditions of the inner region of the annulus the same as those for a heated circular tube. An outline of the method for the heat-transfer data is given in Appendix 1, and the effects in a typical case are shown in Fig. 6.

14. The transformation of the smooth-surface heat-transfer data gives a Nusselt-number correlation similar to the accepted one for turbulent flow in circular tubes, except that the constant 0·023 is replaced by 0·020. This decrease of the constant agrees with observations made by Ede [15]. Similarly the friction-factor data can be transformed, and the remainder of the presentation of results refers to transformed data.

15. Fig. 7 shows the heat-transfer results on a Stanton number–Reynolds number plot, and Fig. 8 gives the friction factors.

16. The velocity-distribution data for the region inside the zero shear boundary are presented in the usual plot of u^+ against y^+; Fig. 9 gives the results for the smooth surface and Fig. 10 for the roughened surface with wire height of 0·040 in. The agreement with the universal velocity-distribution law for a smooth surface is reasonable, particularly if the slopes are compared, although there is a Reynolds-number effect. Using the shear-stress distributions given for the annulus in Fig. 11 [16] the results for all the surfaces are plotted in Fig. 12 to illustrate the velocity defect law.

17. The temperature-distribution data are plotted in Fig. 13 in a similar way to the velocity data.

ANALYSIS OF HEAT-TRANSFER RESULTS

18. In the semi-theoretical analyses of roughened-surface heat transfer presented in references [7] and [9], one concept was developed in similar ways. Briefly, this consisted of dividing the heat-transfer resistance into two parts: an inner region enveloping the tips of the roughness protrusions, and a central region in which it was assumed that Reynolds analogy was obeyed. The analysis of the present data follows the same line of thinking.

19. The temperature at the boundary of the regions is taken as t_1, and the temperature differences can be made non-dimensional in a similar way as velocity differences (see Appendix 2).

20. Writing,

$$(\Delta t^+)_t = (\Delta t^+)_w + (\Delta t^+)_c \qquad (1)$$

where

$$(\Delta t^+)_t = \frac{t_w - t_0}{q/\rho \,.\, u_\tau \,.\, c}, \qquad (\Delta t^+)_w = \frac{t_w - t_1}{q/\rho \,.\, u_\tau \,.\, c}$$

and

$$(\Delta t^+)_c = \frac{t_1 - t_c}{q/\rho \,.\, u_\tau \,.\, c}.$$

21. In the region outside the hypothetical boundary (t_1) the velocity distribution is used to predict the value of $(\Delta t^+)_c$. In evaluating the mean temperature, a "weighting" to allow for the velocity distribution must be applied, and the dimensionless velocity and temperature distributions will be slightly different; the difference is expressed as δm.

$$(t_1 - t_0)^+ \equiv (u_0 - u_1)^+ + \delta m. \qquad (2)$$

22. The value of δm depends on the related velocity and temperature distributions, which in turn depend on the ratio of the eddy diffusivities (ϵ_H/ϵ_M). For example, if $\epsilon_H/\epsilon_M = 1{\cdot}0$, δm is positive, caused by hot fluid near the wall having a low velocity and thus lowering the mean temperature. If ϵ_H/ϵ_M increases, the "weighting" effect explained above remains, but the temperature differences decrease compared to velocity differences in the turbulent core. Consequently δm decreases and can have a negative value.

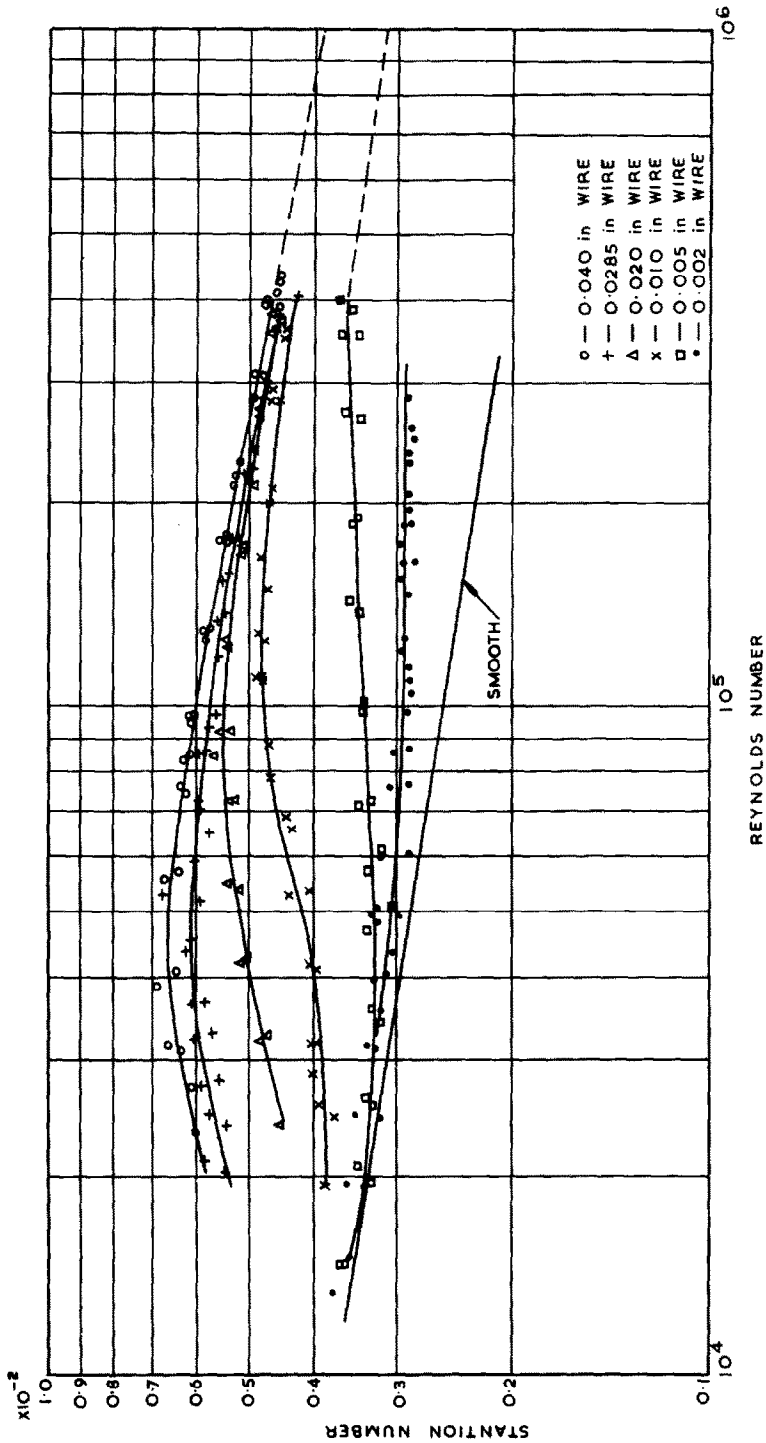

FIG. 7. Transformed Stanton number–Reynolds number plot.

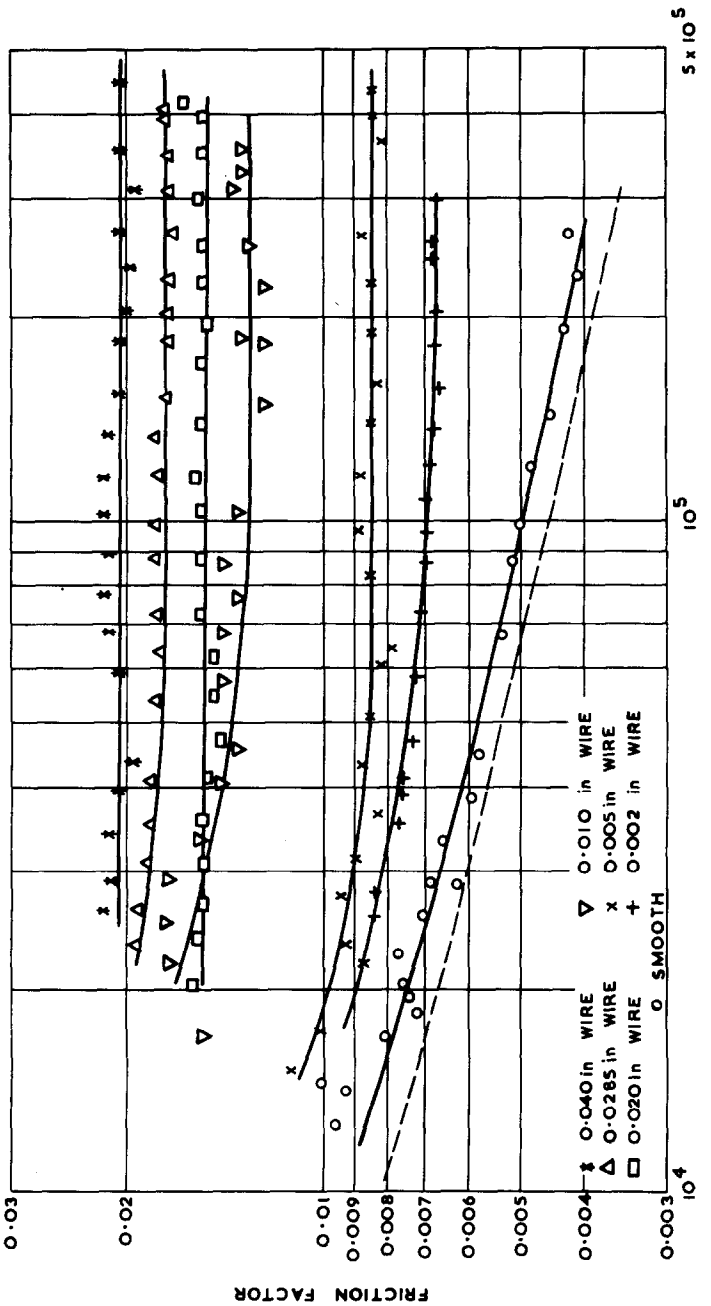

FIG. 8. Transformed friction factors, based on roughness tip area.

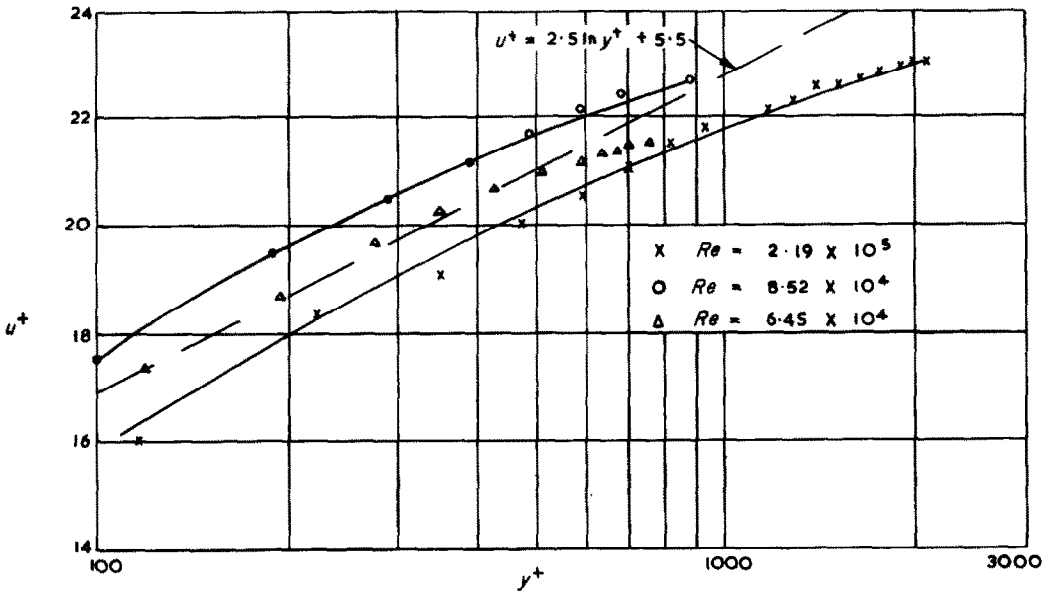

FIG. 9. Universal velocity distribution—smooth surface.

23. Inserting the value of $(t_1 - t_0)^+$ into equation (1),

$$(\Delta t^+)_w = (\Delta t^+)_t - (u_0 - u_1)^+ - \delta m. \quad (3)$$

Now $(\Delta t^+)_t$ is by definition equal to $\sqrt{(f/2)}/St$, and u_0^+ also by definition equals $\sqrt{(2/f)}$; hence equation (3) becomes:

$$(\Delta t^+)_w = \frac{(f/2St) - 1}{\sqrt{(f/2)}} + \frac{u_1}{u_\tau} - \delta m. \quad (4)$$

24. This expression is similar to that used by Dipprey and Sabersky [7], differing only by the inclusion of the correction factor δm. Values of δm were found from the measured velocity and temperature profiles, and since $\epsilon_H/\epsilon_M = 1{\cdot}5$ these were negative.

DISCUSSION OF RESULTS

25. Some comments are made on the overall heat-transfer and friction results before the more detailed discussion. The agreement to within 10 per cent of the smooth annular results with the predicted values of Kays and Leung [13] and the agreement of transformed values with circular tube correlations, are both encouraging results and add to the confidence in these semi-theoretical approaches. That the friction factor for the 0·005- and 0·010-in roughnesses do not approach the smooth surface value at low Reynolds number (Fig. 8) is thought to be caused by the definition of equivalent diameter. Basing the equivalent diameter on the actual surface shape, and not the enveloping cylinder around the roughnesses, the friction factors for 0·005 and 0·010 in are more reasonable in the low Reynolds-number region.

26. The roughened-surface velocity-distribution results, of which Fig. 10 is a typical example, can be correlated by an equation of the form:

$$u^+ = 2{\cdot}5 \ln (y/e) + A. \quad (5)$$

27. The values of A for all the surfaces are shown in Fig. 14 as a function of e^+. At the higher values of e^+ (> 70), A is constant at a mean value of 4·65. This is different from the value of 8·5 obtained by Nikuradse [8, 22] for sandgrain type roughnesses, which is not surprising since A has never been expected to be a universal constant.

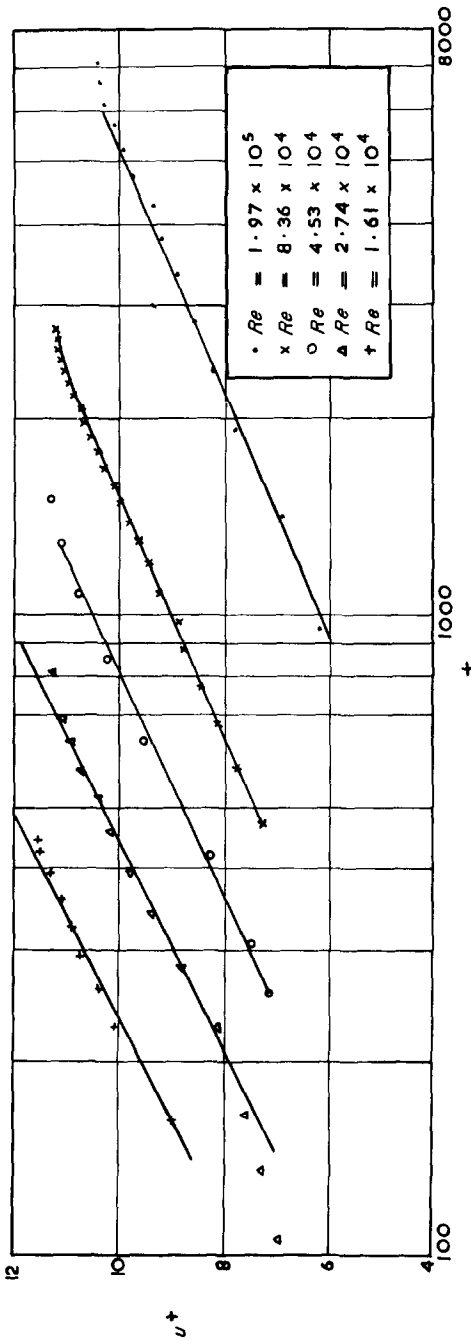

FIG. 10. Universal velocity distribution—0·040-in roughness.

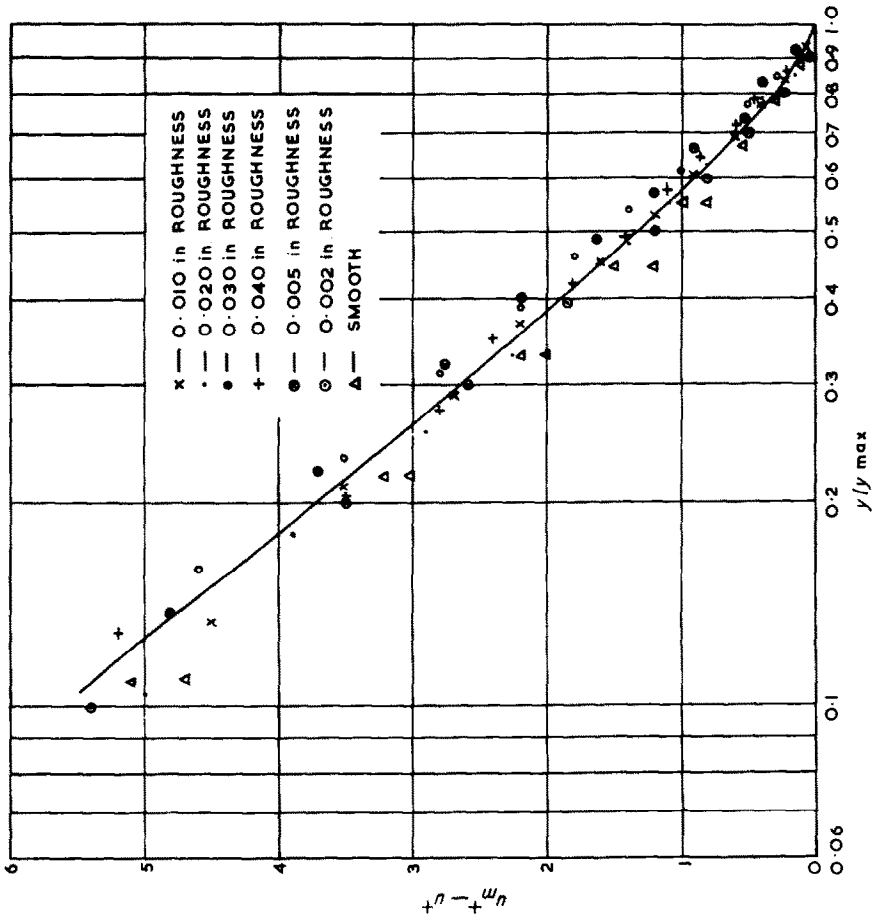

FIG. 12. "Velocity defect" plot of velocity data.

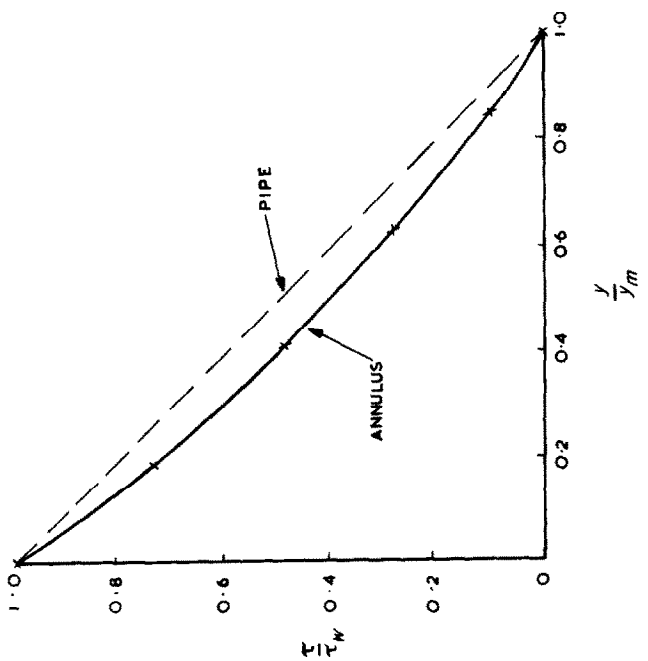

FIG. 11. Shear stress distribution in annulus.

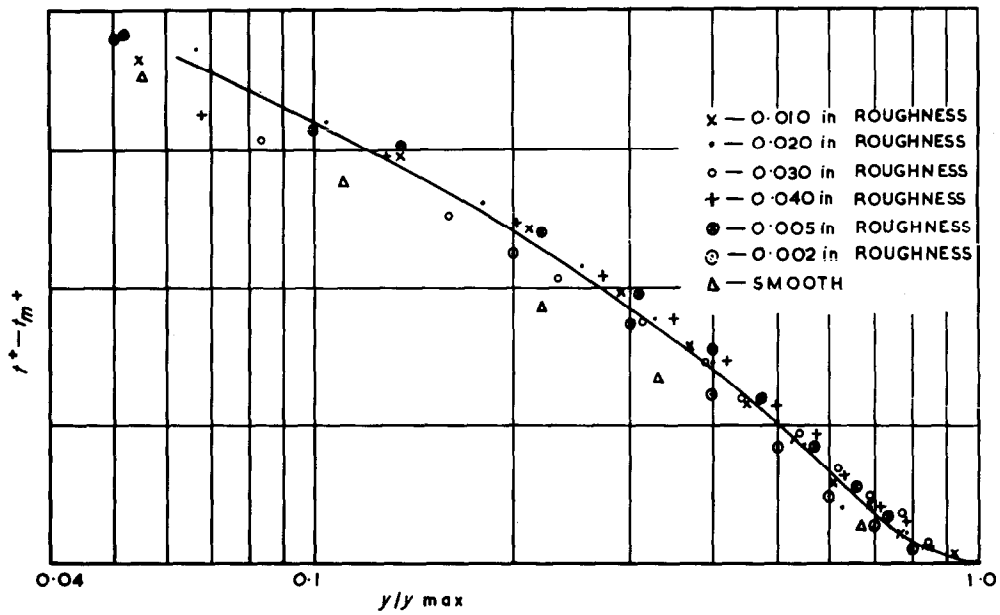

FIG. 13. Temperature distribution away from wall.

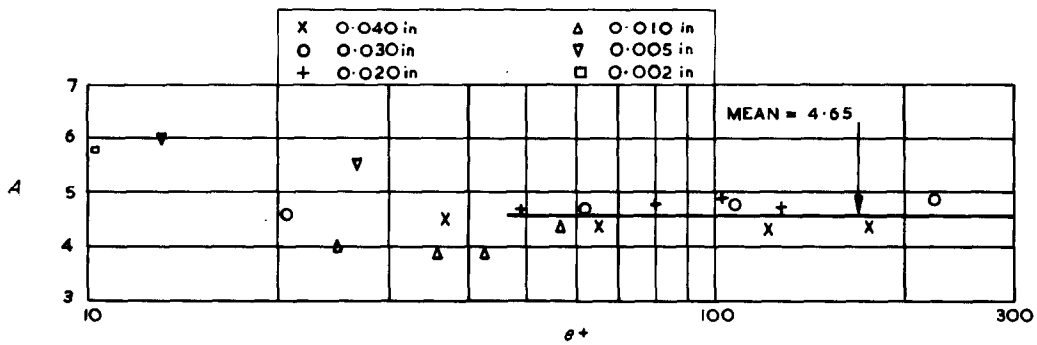

FIG. 14. Variation of A with e^+.

28. Comparing the velocity and temperature profiles shown in Figs. 12 and 13, a value for ϵ_H/ϵ_M can be found since the heat-flux and shear-stress distributions in the central region of the flow will be similar. The value of ϵ_H/ϵ_M obtained is 1·5 which appears to be on the high side, but Larkin [17] has also measured values as large as this.

29. Initially the heat-transfer results were assumed to correlate in terms of h_R/h_s and e^+ with a simple curve giving a constant value of h_R/h_s at large values of e^+ (Fig. 15). Studying the results in detail showed that the smaller roughnesses did not correlate at low e^+, and that the value of h_R/h_s was not constant with e^+ at the higher values.

30. A more detailed analysis of the results has been made, and this is outlined in the preceding section. Basically a correlation of the wall Stanton number $[= (\Delta t^+)_w^{-1\cdot0}]$ with e^+ has been found. The value of Δt_w^+ was found from equation (4) in which the overall heat-transfer and friction values are used together with (u_1/u_τ) and δm. From equation (5), u_1/u_τ

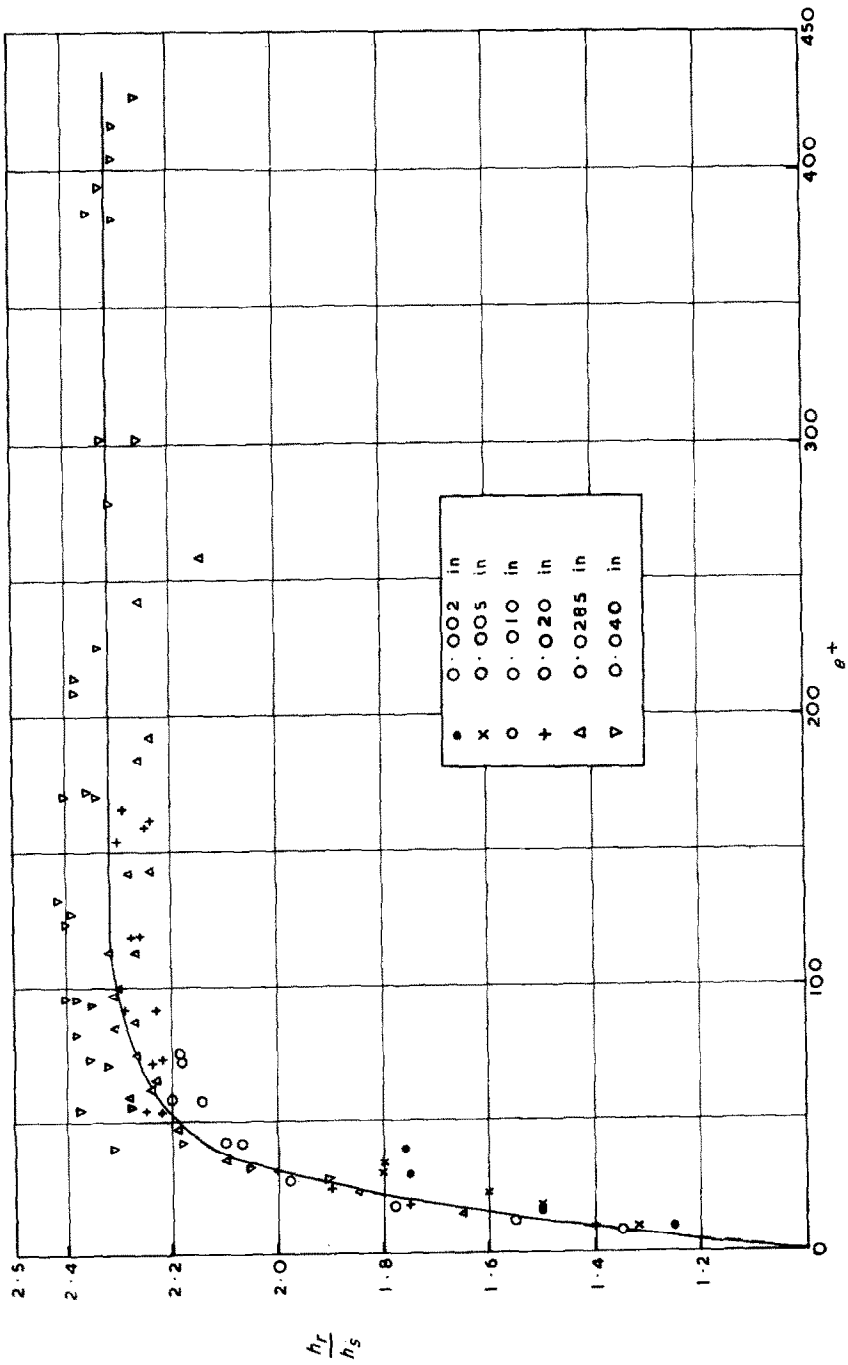

FIG. 15. h_r/h_s against e^+.

is equal to A, and the values of δm were obtained from the velocity and temperature profiles and varied between $-1{\cdot}4$ and $-2{\cdot}1$. The results for the roughened surfaces for $e^+ > 50$ are shown in Fig. 16 and the best-fit line is:

$$\Delta t^+ = (St_w)^{-1{\cdot}0} = 5{\cdot}37\,(e^+)^{0{\cdot}199}. \qquad (6)$$

31. These results are all in the "fully roughened" regime, i.e. $e^+ > 50$. In Fig. 17 the results at lower values of e^+ are presented in a similar manner, and a reasonable correlation is obtained. The absolute value of St_w, however, is open to question at the lower e^+ values since from Fig. 14 it is not clear that the value of A below $e^+ = 50$ remains at 4·65. There is every indication from Nikuradse's work on sand-grain roughnesses that A does correlate with e^+ in this region, but not enough information is available in Fig. 14 to reveal the variation for the roughnesses used in the present investigation. For the values of St_w shown in Fig. 17 it has been assumed that $A = 4{\cdot}65$, and since at $e^+ = 5$ the value of A will tend to 5 for agreement with a smooth surface, any error is likely to be small.

32. The general pattern of Fig. 17 indicates that there are two regimes bounded by $e^+ \sim 35$, at which value the magnitude of St_w reaches a maximum. As would be expected, this maximum coincides with the maxima for the overall Stanton number shown in Fig. 7. It is considered that only a correlation in the "fully rough" regime at $e^+ > 50$ is possible from the experimental results, and no attempt has been made to extend this correlation to lower values of e^+.

33. For the regime with $e^+ > 50$ the overall Stanton number can be obtained from:

$$\frac{1}{St} = \sqrt{\left(\frac{2}{f}\right)}\left[\sqrt{\left(\frac{2}{f}\right)} + \frac{1}{St_w} + \delta m - 4{\cdot}65\right]. \qquad (7)$$

34. Use of equation (7) for the overall Stanton number involves:

(a) Estimating the friction factor
(b) Calculation of St_w from equation (6)
(c) Estimating δm, which for the present purposes can be taken as the mean measured in these tests, i.e. $-1{\cdot}8$.

35. Equation (7) has been used to extrapolate the experimental results in Fig. 7, and these are shown by dotted lines.

36. In comparing the results with those of other workers it is only profitable to make the comparison when the velocity and temperature profiles are also quoted. Only under these

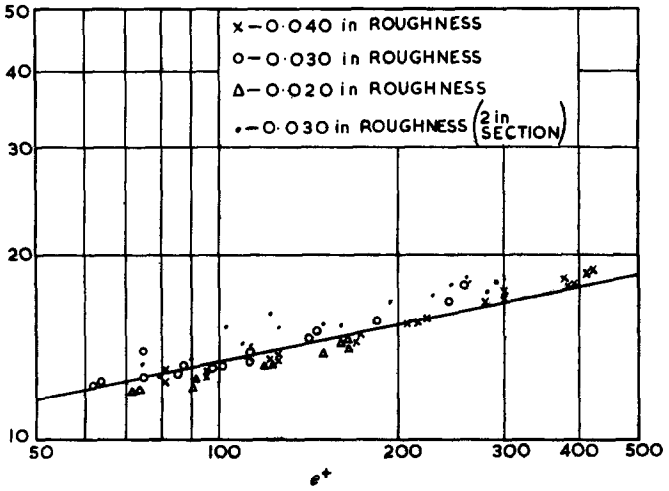

FIG. 16. Correlation of wall Stanton number, vertical axis, with e^+.

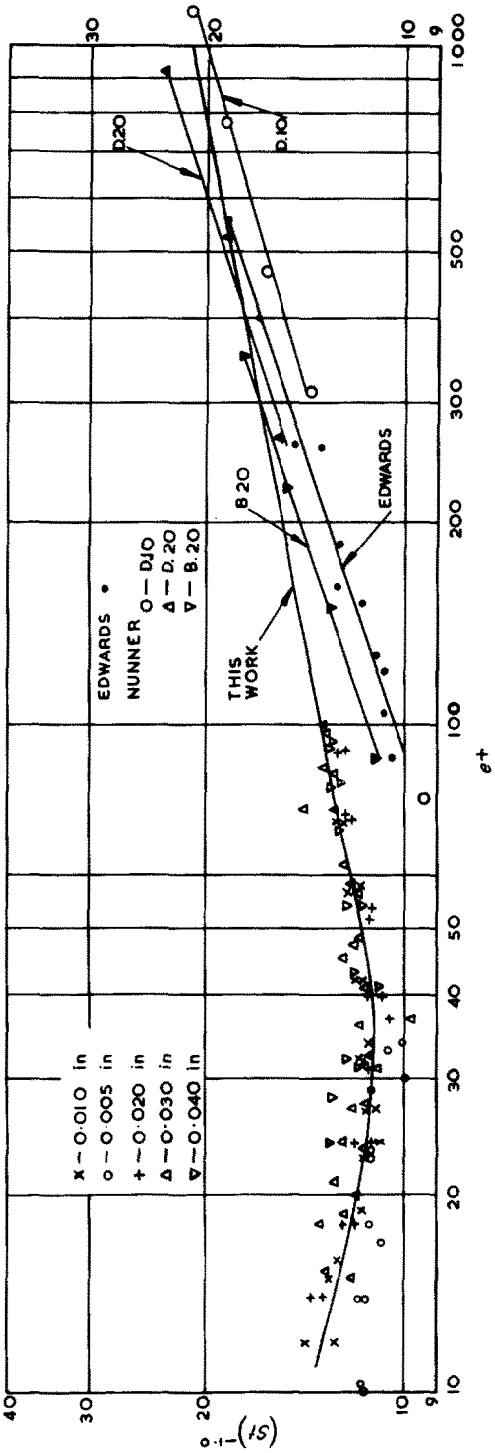

FIG. 17. Correlation of wall Stanton number for full range of e^+.

conditions can the value of St_w be evaluated. Such details were given by Edwards in his study of square-sectioned roughnesses at a pitch-to-height ratio of 15 in a rectangular channel [18]. The velocity distributions gave values of $A \sim 4{\cdot}5$, which compares with the present value of 4·65, and the values of St_w are plotted in Fig. 17. Whilst the absolute values differ, being actually lower (possibly because of the larger pitching and shape), the form of the correlation is similar to that of the present results. Also included in Fig. 17 are the results of Nunner [6] for a tube roughened with semi-circular rings with pitch-to-height ratios of 10 and 20. The value of A obtained from Nunner's velocity data was $\sim 4{\cdot}0$, and the values of St_w are shown on Fig. 17. It was necessary to assess δm from the experimental results. The form of the results is similar to that of the present results, but as with the results of Edwards [18] the absolute value and the slopes are different. These differences emphasize the effects of different configurations, which must be evaluated experimentally.

37. The existence of the maximum in the Stanton number for each roughened surface indicates that there is an optimum heat-transfer condition for each surface. This is discussed in more detail in Appendix 3 together with the application of roughened surfaces. It is shown that the characteristics of a roughened surface necessary to give less pumping power, for the same heat generation and surface–fluid temperature difference in the channel, are:

$$\frac{f_r}{f_s} < \left(\frac{St_r}{St_s}\right)^3.$$

38. Since the results plotted in Fig. 18 show that

$$\frac{f_r}{f_s} < \left(\frac{St_r}{St_s}\right)^2,$$

these roughened surfaces could be used beneficially in the simple example considered.

CONCLUSIONS

39. The important conclusions from the present work are:

(a) A correlation of the heat-transfer results for a given configuration of roughened surface is possible once the roughness has become fully effective. The limit for the effectiveness of the roughness is $e^+ \sim 50$, and the correlating equation is:

$$\frac{1}{St} = \sqrt{\left(\frac{2}{f}\right)}\left[\sqrt{\left(\frac{2}{f}\right)} + \frac{1}{St_w} + \delta m - 4{\cdot}65\right].$$

(b) The wall heat-transfer resistance, $1/St_w$, has a minimum value at $e^+ \sim 35$ which produces an optimum heat-transfer condition.

(c) The improved heat-transfer characteristics of roughened surfaces produce a more efficient heat-transfer surface, despite the increased friction factor (Appendix 3).

ACKNOWLEDGEMENTS

Mr. J. Maddock assisted with the experimental work, and computing effort was provided by Central Technical Services, Risley.

This paper is published by permission of the Managing Director of the Reactor Group of the United Kingdom Atomic Energy Authority.

REFERENCES

1. W. F. Cope, The friction and heat-transmission coefficients of rough pipes, *Proc. Instn Mech. Engrs*, **145**, 99 (1941).
2. Experimental investigation of average heat-transfer and friction coefficients for air flowing in circular tubes having square-thread-type roughnesses, NACA RM E52 D17 (1952).
3. E. W. Sams, Heat transfer and pressure drop characteristics of wire-coil-type turbulence promoters, USAEC Reactor Heat Transfer Conference (1956).
4. A. Draycott and K. R. Lawther, Improvement of fuel element heat transfer by use of roughened surfaces and the application to a 7-rod cluster, International Heat Transfer Conference, University of Colorado, Boulder (1961).
5. V. Walker and A. C. Rapier, AGR symposium on fuel element heat transfer, *J. Br. Nucl. Energy Soc.* **2**, 2 (1963).
6. W. Nunner, Heat transfer and pressure drop in rough

tubes, UKAEA Translation AERE Lib/Trans, 786 (1956).
7. D. F. DIPPREY and R. H. SABERSKY, Heat and momentum transfer in smooth and rough tubes at various Prandtl numbers, *Int. J. Heat Mass Transfer* **6**, 5 (1963).
8. J. NIKURADSE, Laws of Flow in Rough Pipes, VDI Forsch-Heft 361 (1933).
9. P. R. OWEN and W. R. THOMSON, Heat transfer across rough surfaces, *J. Fluid Mech.* **15**, 3 (1963).
10. F. J. EDWARDS and N. SHERIFF, The heat-transfer and friction characteristics for forced-convection heat flow over a particular type of rough surface, International Heat Transfer Conference, University of Colorado, Boulder (1961).
11. N. KATCHEE and W. V. MACKEWICZ, Effects of boundary-layer turbulence promoters on the local film coefficients of Mk 1 fuel elements, *Nucl. Sci. Engng* **16**, 1 (1963).
12. D. W. SAVAGE and J. E. MYERS, The effect of artificial structure roughness on heat and momentum transfer, *A.I.Ch.E. Jl* **9**, 5 (1963).
13. W. M. KAYS and E. Y. LEUNG, Heat transfer in annular passages; hydrodynamically developed turbulent flow with arbitrarily prescribed heat flux, *Int. J. Heat Mass Transfer* **6**, 6 (1963).
14. W. B. HALL, Heat transfer in channels composed of rough and smooth surfaces, *J. Mech. Engng Sci.* **4**, 287 (1962).
15. A. J. EDE, The heat-transfer coefficient for flow in a pipe, *Int. J. Heat Mass Transfer* **4**, 12 (1961).
16. A. C. RAPIER, Forced-convection heat transfer in passages with varying roughness and heat flux around the perimeter, UKAEA, TRG Report 519 (W) (1956).
17. B. S. LARKIN, Ph.D. Thesis University of London, Faculty of Engineering (1961).
18. F. J. EDWARDS, The correlation of forced-convection heat transfer data from surfaces with large-scale roughness, Institution of Mechanical Engineers Thermodynamics and Fluid Mechanics Convention, April 1964, Paper 22 (1964).
19. I. B. BURGOYNE, P. BURNETT and D. WILKIE, Forced-convection heat transfer from surfaces roughened by transverse ribs, UKAEA, TRG Report 781 (W) (1964).
20. E. FOURNEL, On a method of improving heat exchange by forced convection (region of turbulent flow), IV Congrès International du Chauffage Industriel, Paris, groupe 1, section 13, No. 55. (UKAEA Translation AERE Lib/Trans 659.) (1952).
21. R. T. LANCET, The effect of surface roughness on the convection heat-transfer coefficient for fully developed turbulent flow in ducts with uniform heat flux, *J. Heat Transfer, Trans. A.S.M.E. Series C* **81**, 168 (1959).
22. H. SCHLICHTING, *Boundary Layer Theory*. Pergamon Press, London (1956).

APPENDIX 1

Transformation of Heat-transfer Data

In 1962 Hall [14] introduced a transformation particularly for annular passages with only the core tube heated and roughened. Essentially the temperature profile is transformed such that at the position of zero shear stress the heat flux is made zero. Briefly this is achieved by first calculating the effective conductivity up to the zero shear position from the measured velocity and temperature profiles. With the known heat flux, effective conductivity and velocity profile, a temperature profile making the heat flux zero at the zero shear position can be calculated. Using this temperature profile a transformed heat-transfer coefficient can be calculated. Since detailed velocity and temperature transverses are required to apply the transformation, the present study was reduced to about five transverses per roughness over the full Reynolds-number range. The ratios of the transformed to the untransformed heat-transfer coefficients are given in Table 2.

APPENDIX 2

Dimensionless Temperature Distributions

Just as the velocity distribution can be

Table 2. The ratio of the transformed to the untransformed heat-transfer coefficient

Surface	Smooth	0·002-in wire	0·005-in wire	0·010-in wire	0·020-in wire	0·0285-in wire	0·040-in wire
	1·088	1·100	1·111			1·094	1·088
Increasing	1·086	1·099	1·089	1·091	1·086	1·089	1·082
Reynolds	1·099	1·080	1·089	1·086	1·069	1·082	1·076
number ↓	1·078	1·107	1·076	1·087	1·075	1·071	1·069
		1·084		1·081	1·069	1·056	

analysed by making the velocity dimensionless by dividing by the friction velocity $\sqrt{(\tau/\rho)}$, so too can the temperature distribution. If we consider the fully turbulent core, the heat flux and shear stress, respectively, are given by:

$$q = -c\rho\epsilon_H \frac{dt}{dy}$$

$$\tau = \rho\epsilon_M \frac{du}{dy}.$$

Dividing these two equations gives:

$$\frac{(dt/dy)\,\rho c\epsilon_H}{(du/dy)\,\rho\epsilon_M} = -\frac{q}{\tau}. \tag{8}$$

Simplifying this and expressing $du/\sqrt{(\tau/\rho)}$ as Δu^+ we obtain:

$$dt = \frac{\epsilon_M}{\epsilon_H} \cdot \frac{q}{\rho c\sqrt{(\tau/\rho)}} \cdot \Delta u^+.$$

Now $q/\rho c\sqrt{(\tau/\rho)}$ has dimensions of temperature and can be used to make dt dimensionless; therefore equation (8) becomes:

$$\Delta t^+ = \frac{\epsilon_M}{\epsilon_H} \Delta u^+$$

where

$$\Delta t^+ = -\frac{dt}{q/\rho c\sqrt{(\tau/\rho)}}.$$

This expresses the fact that temperature and velocity distribution in the turbulent core are identical if the eddy diffusivities of heat and momentum are equal.

APPENDIX 3

Application of Roughened Surfaces

From the experimental results the increase in the friction factor is greater than the increase in the Stanton number for roughened surfaces. This result agrees with those of most roughened-surface studies. For a smooth surface, a significant part of the fluid resistance and heat-transfer resistance occurs in the region near the wall. The thickness of the laminar boundary layer and the molecular properties of the fluid determine the magnitude of these resistances to the transport of heat and momentum. Conditions for a roughened surface are different, in that the high shear stress in the fluid is the result of form drag on the roughness elements. Consequently, despite the increase in the friction factor, there is not a region near the wall where this increased shear stress is transported by means of the viscosity of the fluid alone, which would result in a limitation because of the fluid viscosity. The transportation of heat, on the other hand, is still limited by the thermal conductivity of the fluid adjacent to the wall. These differences between smooth and roughened surfaces are such that it is not to be expected that Reynolds analogy holds for roughened surfaces.

In analysing the expected effect of increasing the friction factor, it is useful to consider the turbulent velocity component derived from the definition of the friction factor, namely $u_\tau = u\sqrt{(f/2)}$. In broad terms this velocity determines the eddy diffusivity in the core of the flow and the thickness of any laminar sub-layer. For smooth surfaces the value of u_τ increases as the Reynolds number increases, because of the increase in u, and the heat transfer correspondingly increases. For roughened surfaces the value of u_τ increases because of the increase in f, and thus the heat transfer increases. These simple considerations show that the same increase in the heat-transfer coefficient can be obtained for either a smooth surface with a higher velocity, or a roughened one with a higher friction factor. Whichever method is used, the shear stress at the wall, and hence the pressure drop, will be the same. For a smooth surface, however, more energy is dissipated in the process of increasing h, since the increase in u_τ applies to more fluid per unit of time. The roughened surface can thus be considered as a more efficient way of increasing the heat-transfer properties of the surface, and the following example underlines the above argument.

Let L = length,
d = diameter,
V = fluid velocity,
$(\Delta T)_R$ = fluid temperature rise,
ΔT = surface-fluid temperature difference.

Now

$$St = \frac{(\Delta T)_R}{\Delta T} \cdot \frac{d}{4L}.$$

Total heat output from channel,

$$Q = \rho V c \frac{\pi d^2}{4} (\Delta T)_R$$
$$= \rho V c \, \pi d L \, St \Delta T.$$

Pumping power for fluid,

$$P = \tfrac{1}{2} \rho V^2 f \frac{4L}{d} V \frac{\pi d^2}{4}$$
$$= f V^3 \frac{\pi d L}{2} \rho.$$

Ratio of the pumping power to the heat output in the channel is:

$$\frac{f V^2}{(2c\Delta T)\, St}.$$

Consider increasing the power in the channel for the same surface–fluid temperature difference. The ratio P/Q is proportional to

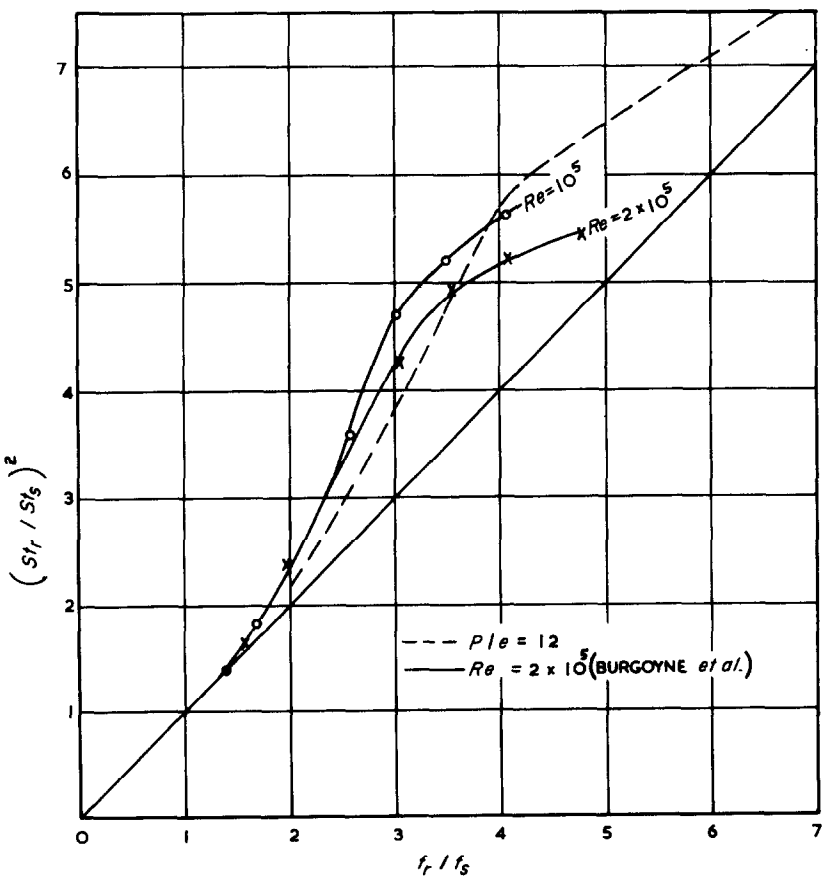

FIG. 18. Comparison of roughened surface in terms of (St_r/St_s) and (f_r/f_s).

fV^2/St. If a smooth surface is used, let the velocity be increased to V_1. For the same heat output for a roughened surface, $St_r/St_s \simeq V_1/V$, and the condition for less pumping power for the roughened surface is:

$$\frac{f_r}{St_r} V^2 < \frac{f_s}{St_r} V_1^2$$

or

$$\frac{f_r}{f_s} < \frac{St_r}{St_s} \frac{V_1^2}{V^2}$$

or

$$\frac{f_r}{f_s} < \left(\frac{St_r}{St_s}\right)^3.$$

Thus, if it is required to double the power output of the channel, the roughened surface must be such that $St_r/St_s = 2$ and $f_r/f_s < 8$. These conditions are easily met for the surfaces studied; in fact $f_r/f_s < (St_r/St_s)^2$ as is shown in Fig. 18.

Whilst this example has been simplified, the general principle applies in the more rigorous use of roughened surfaces.

From Fig. 18 the optimum surface would occur at a value of f_r/f_s of about 3, since at greater values the rate of increase in Stanton number is reduced. The reason for the optimum follows from the maximum value of Stanton number on the *St–Re* plot of Fig. 7, which has been explained in terms of a maximum value of the wall Stanton number at $e^+ \sim 35$. A similar optimum is obtained from the results of Burgoyne *et al.* [19] when plotted on Fig. 18. Although this work is not directly comparable, since the pitch-to-height ratio was 12 and the cross-section of the roughness was square, the existence of a similar optimum surface is encouraging to the present analysis.

Résumé—Les caractéristiques de transport de chaleur et de frottement d'une surface avec des rugosités distinctes ont été étudiées expérimentalement.

Les surfaces ont été rendues rugueuses au moyen d'un fil enroulé avec un rapport constant du pas au diamètre du fil de 10:1, avec des diamètres de fil variant de 0,05 mm à 1 mm.

On a trouvé utile une corrélation simple basée sur un paramètre de rugosité sans dimensions e^+, mais une corrélation basée sur un modèle à deux couches de la résistance au transport de chaleur était plus exacte. Dans ce modèle, le processus de transport de chaleur était divisé en une région allant de la paroi à l'enveloppe des sommets des rugosités et une région centrale.

La résistance au transport de chaleur de la paroi aux extrémités des rugosités a une valeur minimale pour $e^+ \sim 35$, et ceci correspond à une surface optimale de transport de chaleur.

Zusammenfassung— Wärmeübergang und Reibungscharakteristika an Oberflächen mit besonderen Rauhigkeiten wurden experimentell untersucht.

Die Oberflächenrauhigkeit wurde durch eine Drahtbewicklung erzielt mit einem konstanten Verhältnis 10:1 von Steigung zu Drahtdurchmesser bei verschiedenen Drahtdurchmessern von 0,05 bis 1 mm.

Eine einfache Beziehung auf Grund des dimensionslosen Rauhigkeitsparameters e^+ erwies sich als nützlich; eine, auf dem Zweischichtenmodell des Wärmeübergangswiderstandes beruhende Korrelation zeigte sich jedoch als genauer. Bei diesem Modell wurde der Wärmeübergang unterteilt für einen Bereich von der Wand bis zur Umhüllenden um die Rauhigkeitsspitzen und für einen zentralen Kernbereich.

Der Wärmeübergangswiderstand von der Wand zu den Rauhigkeitsspitzen hat ein Minimum bei $e^+ \sim 35$; dafür ergibt sich eine optimale Wärmeübergangsfläche.

Аннотация—Проведено экспериментальное исследование теплообмена и трения на поверхности с распределенной шероховатостью.

Шероховатость поверхности создавалась проволокой, при чем отношение шага витка к диаметру было 10 : 1, а диаметр проволоки изменялся от 0,002 до 0,040 дюймов.

Установлено, что результаты экспериментов можно обобщить с помощью безразмерного параметра шероховатости e^+, однако лучшее совпадение достигается применением обобщенного соотношения на основе двухслойной модели. В этой модели процесс

теплообмена делится на две области: участок между стенкой и вершинами элементов шероховатости и центральную часть потока.

Минимум теплообмена в области между стенкой и вершинами элементов шероховатости соответствует $e^+ \sim 35$, что позволяет создать оптимальную поверхность теплообмена.